inorganics

MDPI

Article

Ketone Formation via Decarboxylation Reactions of Fatty Acids Using Solid Hydroxide/Oxide Catalysts

Benjamin Smith [1,2], Li Li [1,2], Diego D. Perera-Solis [1,2], Louise F. Gildea [1,2], Vladimir L. Zholobenko [3], Philip W. Dyer [1,2,*] and H. Christopher Greenwell [1,4,*]

1 Centre for Sustainable Chemical Processes, Department of Chemistry, Durham University, Durham DH1 3LE, UK; benjamin.smith@dunelm.org.uk (B.S.); li.li2@durham.ac.uk (L.L.); diego.d.perera-solis@durham.ac.uk (D.D.P.-S.); lfgildea@gmail.com (L.F.G.)
2 Department of Chemistry, Durham University, Durham DH1 3LE, UK
3 Lennard-Jones Laboratories, Keele University, Staffordshire ST5 5BG, UK; v.l.zholobenko@keele.ac.uk
4 Department of Earth Sciences, Durham University, Durham DH1 3LE, UK
* Correspondence: p.w.dyer@durham.ac.uk (P.W.D.); chris.greenwell@durham.ac.uk (H.C.G.); Tel.: +44-191-334-2150 (P.W.D.); +44-191-334-2324 (H.C.G.)

Received: 30 August 2018; Accepted: 19 October 2018; Published: 8 November 2018

Abstract: A sustainable route to ketones is described where stearone is produced via ketonic decarboxylation of stearic acid mediated by solid base catalysts in yields of up to 97%, at 250 °C. A range of Mg/Al layered double hydroxide (LDH) and mixed metal oxide (MMO) solid base catalysts were prepared with Mg/Al ratios of between 2 and 6 via two synthetic routes, co-precipitation and co-hydration, with each material tested for their catalytic performance. For a given Mg/Al ratio, the LDH and MMO materials showed similar reactivity, with no correlation to the method of preparation. The presence of co-produced oxide phases in the co-hydration catalysts had negligible impact on reactivity.

Keywords: base catalysis; mixed metal oxide; layered double hydroxide; liquid phase; ketonisation; biorefinery; fatty acid

1. Introduction

Crude oil is a finite feedstock and attempts are being made to extend the shelf life of infrastructure and chemical processes that rely on its use by producing sustainable bio-derived fuels and chemicals [1,2]. For example, certain seeds, plants, and algae can be processed to afford oils, where the majority of the non-polar oil components are in the form of triacyl glycerides (TAGs), consisting of an ester of glycerol bearing three saturated or unsaturated fatty acid residues [3]. These TAGs can be readily hydrolysed to form glycerol, itself a potential source of fuels and chemicals, and free fatty acids (FFA) [4]. The resulting FFAs can be treated in a number of ways to afford a range of valuable chemical products such as diesel-like fuels, lubricants and gasoline [5,6]. A particularly important derivatisation pathway is ketonic decarboxylation (or ketonisation), whereby two carboxylic acid molecules react to form a ketone with loss of water and carbon dioxide. Depending on the nature of the starting carboxylic acids, the resulting FFA-derived ketones are potentially useful, environmentally-sustainable feedstocks for use in diesel fuels, lubricants, as surfactant precursors, or as substrates for further functionalisation, for example, via cracking or hydrotreatment to afford hydrocarbons and hydroxyalkylenes [7,8]. A simple example of a ketonic decarboxylation reaction and a proposed mechanism is presented in Figure 1. Here, a solid ceria catalyst was used to convert acetic acid (used as a model FFA) to acetone [9].

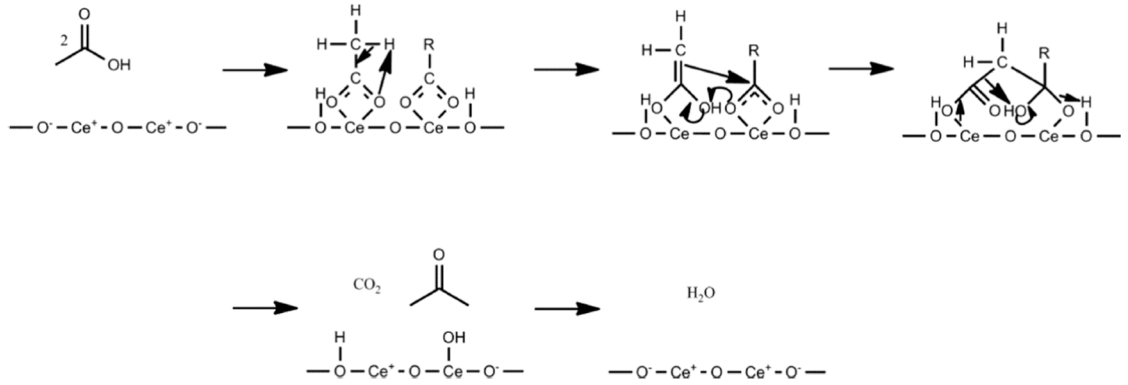

Figure 1. Possible ketonisation mechanism for acetic acid over CeO_2 catalyst. Modified with permission from Snell and Shanks [9] published by American Chemical Society, 2013.

Despite the potential of the ketonisation reaction, today long chain ketone production is still mainly achieved via oxidation of fossil-derived hydrocarbons, something that is unsustainable [10]. Consequently, several underpinning studies have probed the use of heterogeneous catalysts for the preparation of ketones from FFAs and model FFAs using a ketonic decarboxylation approach. For example, Deng et al. explored catalytic ketonic decarboxylation of acetic acid using a range of weakly basic metal oxides on different support materials, finding ceria and manganate supported on silica as being particularly efficient, with conversions close to 100% [11]. In a related study, Nagashima et al. successfully demonstrated ketonic decarboxylation of propanoic acid using CeO_x-based composite oxides [12]. Shutilov and co-workers researched the production of 5-nonanone from pentanoic acid using different zirconium catalysts and found that CeO_2-ZrO_2 yielded maximum conversion and selectivity of 93.2% and 78.7%, respectively [13]. A comprehensive study of ketonic decarboxylation from hexanoic acid mediated by weakly basic ceria/zirconia catalysts was undertaken by Gaertner and colleagues [14]. Here, the activation energy (132 kJ·mol^{-1}) was identified as being significantly higher than that for the esterification reaction (40 kJ·mol^{-1}), such that the irreversible ketonic decarboxylation was favoured at temperatures above 300 °C.

As already indicated, studies around ketonic decarboxylation have been undertaken using acetic acid as the substrate since this acid is representative of low molecular weight acids found in complex biomass-derived oil mixtures. However, these studies have clearly exemplified that the nature (e.g., chemical composition, method of preparation, process conditions, etc.) of the catalyst employed have a very pronounced impact on the ketonisation process. For example, Deng et al. obtained a conversion of 97.3% of acetic acid using a CeO_2 catalyst supported on silica after 96 h at 450 °C [11]. In contrast, Snell and Shanks [9] reported full conversion of acetic acid over a ceria catalyst with reaction temperatures over 300 °C, whereas Yamada et al. [15] working also with a ceria-based catalyst achieved a conversion of 51.3% at 350 °C. In a related study targeting the synthesis of a specific asymmetric ketone fragrance compound, 2-undecanone, Jackson and Cermak successfully ketonised oil from the plant *Cuphea sp*. with acetic acid using a mixed oxide based on Fe/Ce/Al, achieving a 91% yield with reaction temperatures in excess of 300 °C [16].

Mechanistic studies have demonstrated that the ketonic decarboxylation reaction occurs only when an acidic hydrogen is present in the α-position to the carboxylate group, something required to generate the necessary enolate species (see Figure 1) [17–21]. In an attempt to understand the reactivity of carboxylic acids at zirconia surfaces, and the enolization of carboxylates (the mechanism and energy required for the α-hydrogen abstraction and to determine whether enolization is part of the ketonisation mechanism), Ignatchenko undertook density functional theory electronic structure simulations of this process [22]. This study demonstrated that, with zirconia, the most important intermediate in the carboxylic acid ketonisation mechanism is indeed the enolate. This originates following surface-mediated α-hydrogen abstraction and subsequent enolization—a process that is shown to have different energies depending on the specific site at zirconia to which the acid is bound

initially and involves formation of a surface ketene intermediate. In a follow-on study, Ignatchenko and Kozliak carried out experimental isotopic labelling studies to probe the mechanism of both symmetric and cross-coupled ketonic decarboxylation reactions, to determine whether enolization is related with the rate-limiting step and what other factors could govern the mechanism of the reaction [23]. Based on their detailed kinetic analysis, the rate-limiting step occurs after the enol component activation and corresponds to the decarboxylation process.

Support for Ignatchenko's proposed surface ketene mechanism, which resembles the enolization of carboxylates, has also been proposed by Randery et al. [24]. In contrast, Pham and co-workers, working on the ketonic decarboxylation of acetic acid, did not observe a ketene intermediate and hence concluded that no such intermediate species was formed during the ketonisation reaction [25]. However, studies by both Corma et al. [18] and Pulido et al. [26] showed that a β-ketoacid mechanism involving α-hydrogens is kinetically favoured over all other pathways. Despite this mechanism's general acceptance, the β-ketoacid decomposes rapidly, something that hinders its observation during the ketonisation reaction [19]. Together, these studies highlight the complexity of oxide surface-mediated ketonisation processes and emphasise the intimate role the catalyst plays in such reactions.

Whereas much of the prior research to date has focussed on the effect of the substrate on the reaction, the role of the catalyst base site strength has been less well studied. As described, various metal oxides mediate catalytic ketonic decarboxylation [27], and depending on the specific oxide being employed, studies have shown that catalytic ketonisation performance can be enhanced by increasing the basicity of poorly basic surface sites (e.g., using an appropriately-prepared Al_2O_3 catalyst) [11] or by increasing the number of surface basic sites (employing either ceria-zirconia or zirconia oxide systems) [14]. Here, we present an investigation of the use of medium-strong solid base catalysts, in the form of layered double hydroxides and their calcined mixed metal oxide products, for the liquid phase ketonic decarboxylation of a long chain fatty acid, stearic acid.

1.1. An Introduction to Layered Double Hydroxides

Layered double hydroxides (LDHs) are a versatile class of host–guest material consisting of positively-charged metal hydroxide layers charge-balanced by anions that reside, along with water, in the interlayer (Figure 2) [28,29]. LDHs are sometimes called anionic clays, as they share similar intercalation chemistry with the ubiquitous cationic clays (e.g., montmorillonite). LDHs have the general composition of $[M^{2+}{}_{1-x}M^{3+}{}_{x}(OH)_2]^{x+}(A^-)_{x/n}\cdot mH_2O$, with one of the most commonly used forms of synthetic LDH being structurally similar to the naturally occurring mineral hydrotalcite ($Mg_6Al_2(OH)_{16}CO_3\cdot 4H_2O$). Various methods for the synthesis of LDH materials have been described and reviewed in recent years [28–31]. The most common strategies for the preparation of such materials include co-precipitation [32], urea hydrolysis [33], precipitation from organic acid salts [34] and, more recently, co-hydration of suitable metal oxides or hydroxides [35,36].

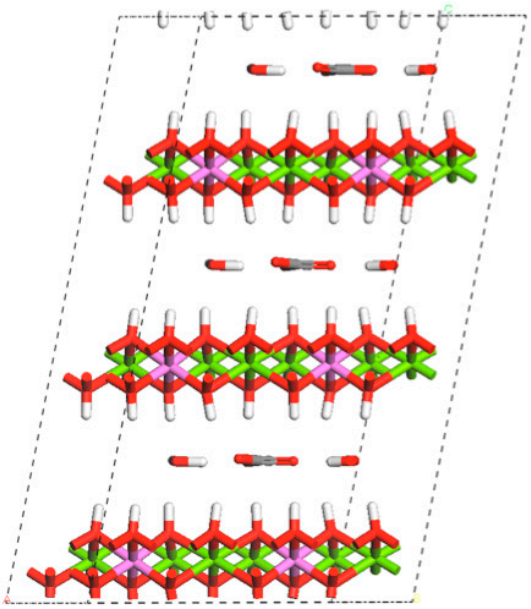

Figure 2. Schematic representation of a carbonate-containing Mg/Al layered double hydroxide super cell showing layered structure and interlayer water. Colour code: Mg = magenta; Al = green; O = red; C = grey; H = white. Dashed lines show periodic cell boundaries.

1.2. Layered Double Hydroxides as Catalysts and Catalyst Precursors

LDHs have been observed to promote a variety of different catalytic reactions. Their versatility has been ascribed both to the presence of different catalytically-active species within their structure (e.g., M–OH, M–O^- in different coordination states in the lattice, as well as OH^- and other charge-balancing ions) and to their ability to perform as both solid acids and/or solid bases [37,38]. The basicity of LDHs is influenced by the M^{2+}/M^{3+} ratio as well as by the anion that is located within the interlayer [39]. For example, catalytic ester hydrolysis has been proposed to take place through reactions occurring at specific LDH lateral crystal faces, whilst *trans*-esterification catalysis is regarded as being less specific, proceeding at a multitude of sites spread across the whole outer LDH crystal surface [40]. The way in which the various LDH materials are activated offers scope to tune these types of system for different catalytic transformations, with calcination and subsequent (partial) rehydration of the resultant to mixed metal oxides (MMOs) having been shown to be an effective method for achieving different basic properties, a topic reviewed by Figueras et al. [41].

In the broader context of heterogeneous catalysis, an important application of LDHs is their use as precursors to MMOs, prepared via calcination. When calcined, LDHs lose the carbonate (or other) interlayer species and undergo dehydroxylation, generating a material that can have a large specific surface area and high porosity, as well as increased basicity, depending on the thermal treatment applied [42,43]. MMOs and rehydrated MMOs have been used as heterogeneous base catalysts in numerous reactions including condensation [44], *trans*-esterification (e.g., for biodiesel production) [45], Michael addition [46], and ketonic decarboxylation [47]. Notably, the rehydrated MMO materials often demonstrate improved catalytic performance compared with that of their LDH precursors [48]. This has been attributed to the MMOs/rehydrated MMOs possessing sites of low (OH^-), medium (O^{2-}–M^{n+}), and high (O^{2-}) basicity [31], together with a regular distribution of the two different metal cations within an oxide matrix [49,50]. For example, Constantino and Pinnavaia studied the relative efficacy of carbonate-containing LDHs compared to partially- (150 °C) and fully-calcined (890 °C) LDHs for the conversion of 2-methyl-3-butyn-2-ol (MBOH) to acetone and ethyne [51]. This study found that LDHs heated at 150 °C, which have lost their intra-pore water, but that still retain interlayer water and carbonate, exhibited greater reactivity (at lower temperature) than materials that had been

calcined previously at 890 °C. According to the authors, although calcination increased the surface area of the compound, intrinsic reactivity was lost.

Importantly, it is now well-established that the exact method of LDH preparation has a significant effect on their performance as catalysts [52]. For example, catalytic efficiency of various different LDH materials has been shown to be enhanced when they are prepared using co-precipitation methods, something proposed to result from the small, high lateral surface area crystals produced under such conditions [29,53]. However, caution is required since it has been clearly demonstrated that residual Na^+/K^+ ions from the necessary base employed during co-precipitation can be retained within the ensuing LDH material, which can significantly affect reactivity, behaving as both homo- and heterogeneous catalysts in their own right [31,52]. In contrast to the high lateral surface area achieved by co-precipitation, high aspect ratio LDHs with high basal surface area may be prepared via hydrothermal synthesis methods, something of particular relevance for applications in composite material preparation [54].

Of particular relevance to the use of LDH materials in catalytic applications is the observation that the strength of the basic sites of both LDHs and post-calcination MMOs can be controlled through variation of the M^{2+}/M^{3+} ratio within the two-dimensional sheet structures; this ratio is denoted as the *R*-value. In studies of ketonic decarboxylation reactions by Parida and Das, which used both LDH materials with various *R*-values and the corresponding MMOs, it was established that an Mg/Al LDH with *R*-value of 4 gave the best conversion of acetic acid to acetone, and that upon its calcination at 450 °C to the corresponding MMO, the catalytic conversion increased further [47]. This enhanced performance of the MMO over that of its parent LDH has been attributed to an increase in the number of strongly basic (O^{2-}) sites post-calcination, something accompanied by an overall reduction in the total number of basic sites, with the lattice Al^{3+} centres providing dual acid-base (amphoteric) character [55]. A study by Xie et al. showed that the greatest basicity (assessed qualitatively using Hammett base indicators [56]) was found with Mg/Al LDH materials having Mg/Al = 3, and that calcination of this material at 464 °C, lead to the optimal performing catalyst for solid base *trans*-esterification [57]. This correlates with other studies where calcined LDHs have been shown to have greater numbers of strongly basic sites than even MgO, a well-established solid base catalyst, though this conflicts with an earlier study where the number and strength of basic sites was reported as greater for MgO than for calcined LDHs [58,59]. However, these reported differences may be attributed to a number of experimental factors that differed between the two studies including synthetic and purification methods (leading to different morphologies and particle sizes).

In summary, it has been reported previously that LDHs and MMOs both perform as effective solid catalysts in a variety of organic transformations, including ketonic decarboxylation. However, to date the bulk of the research effort for this particular transformation has focussed on the use of weakly basic metal-based oxide catalysts. In this paper, we investigate the use of a range of Mg/Al LDHs, and their corresponding MMOs, for the low temperature (250 °C) conversion of stearic acid to stearone via ketonic decarboxylation. The LDHs were prepared by an environmentally friendly co-hydration synthetic route [36], according to well-established green chemical principles, as well as by a more conventional co-precipitation route. One of the advantages of the co-hydration preparation method is that it eliminates the need for strong aqueous alkaline bases essential in traditional co-precipitation methodologies, which remains as waste at the end of the process and which can also initiate catalytic reactions. Furthermore, co-hydration tends to lead to catalysts with high aspect ratio crystals, quite distinct to those achieved via co-precipitation [36].

2. Results

2.1. Structure of Prepared Mixed Metal Oxide Materials

Often when comparing catalytic reactions mediated by LDHs/MMOs it can be difficult to separate the effect of differing variables between studies. For example, it is well established

that a host of parameters can impact considerably on the physicochemical properties of such materials: LDH synthesis method, which can significantly alter product crystallinity/purity; calcination temperatures/conditions; and post calcination treatment. Before undertaking any catalysis studies, the composition and structure of the various Mg/Al LDH materials formed via co-precipitation and co-hydration, together with those of their corresponding mixed metal oxides, were examined. To this end, the catalyst samples are described according to: (i) the method of preparation, CoP = co-precipitation and CoH = co-hydration; (ii) whether LDH or MMO; and (iii) the starting Mg/Al stoichiometry or *R*-value. For example, using this notation a mixed metal oxide prepared via a co-precipitation route with Mg/Al ratio of 4 would be denoted CoP-MMO-4.

2.1.1. Structure and Basicity of Layered Double Hydroxides Prepared by Co-Precipitation

The powder X-ray diffraction (PXRD) patterns obtained for the various LDH materials prepared through co-precipitation (CoP-LDH-2 to CoP-LDH-6) are shown in Figure 3a; a summary of the PXRD data for the CoP-LDH samples is given in Table 1. For each of the materials, the PXRD patterns obtained are characteristic of LDH materials [60,61]. ICP-OES analyses of each of the CoP-LDH materials was used to determine the *R*-values (Table 1). These *R*-values correlated well with the percentage of aluminium present in each LDH phase as determined from the distinct d_{110} LDH reflection, which systematically varies as a function of Al substitution, based on the line of best fit equation proposed by Kaneyoshi and Jones for carbonate and nitrate LDHs [62]. Thermal analysis via thermogravimetric analysis (TGA) of the CoP-LDHs showed the expected distinct mass losses associated with evolution of water, initially from loss of intercalated interlayer water and then from dehydroxylation of the hydroxide layers, and later from carbon dioxide arising from interlayer carbonate decomposition upon calcination from room temperature to 500 °C [63].

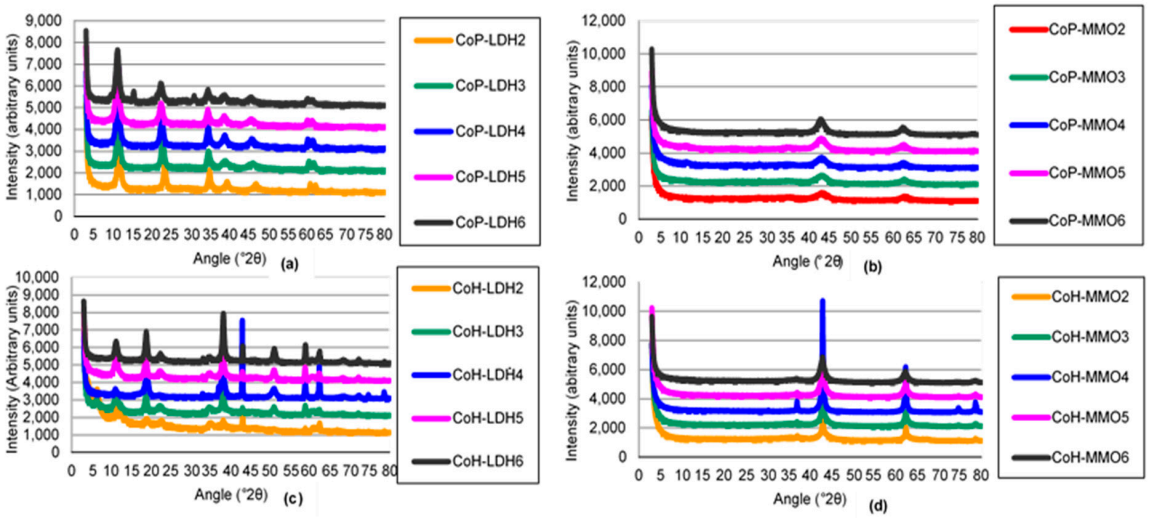

Figure 3. Powder X-ray diffraction patterns for LDH prepared via co-precipitation and their corresponding, thermally-generated MMOs: (**a**) CoP-LDH; (**b**) CoP-MMO; (**c**) CoH-LDH; and (**d**) CoH-MMO.

To assess the potential catalytic performance of each of the prepared LDHs in ketonic decarboxylation, although not easy to achieve in practice, a qualitative investigation of the relative basicity of each of the materials was undertaken. To this end, we attempted to determine the basicity of the various materials using an FTIR probe molecule adsorption/desorption approach, but this proved inappropriate for these very weakly basic materials (see Supplementary Materials). Consequently, an alternative previously-reported methodology was employed, whereby the various LDH and MMO materials were treated with dry methanolic solutions of standard Hammett base indicators (Table 1) [57]. However, it should be noted that, owing to the bulky nature of the molecules used as

Hammett indicators, this approach does not probe the interlayer; instead it provides an estimation of external surface basicity of the layered materials prepared [64]. Qualitatively, the surface basicity of materials CoP-LDH-2, and CoP-LDH-4–CoP-LDH-6 was found to lie in the range pH 9.0–10.0, while that for CoP-LDH-3 was slightly lower, lying in the range pH 7.6–9.0.

A representative SEM image of CoP-LDH-3 is shown in Figure 4a, alongside an LDH prepared by co-hydration (CoH-LDH-2, Figure 4b), both of which display the typical anisotropic layered morphology for an LDH, with the co-hydrated sample visually having a high aspect ratio, as exemplified by the average crystal sizes in the *a* and *c* directions (Table 1). Surface area analyses data were obtained using N_2 adsorption methods and are reported in Table 1. It was found that the surface area of the various materials decreased with decreasing aluminium content for CoP-LDH-2 (91 $m^2 \cdot g^{-1}$) to CoP-LDH-3 (82 $m^2 \cdot g^{-1}$), values that are in line with the typical 100 $m^2 \cdot g^{-1}$ cited for hydrotalcites [31]. In contrast, the surface areas for the related materials CoP-LDH-4 to CoP-LDH-6 were significantly lower (17–39 $m^2 \cdot g^{-1}$), with a slight increase in surface area being found with decreasing Al-content. A similar trend of increasing surface area with increasing Mg–Al ratio has been described previously [65]. The average pore sizes were found to generally increase with decreasing Al-content over the range from ~3 to ~21 nm, although the N_2 adsorption technique used here does not probe the interlayer, but instead relates to inter-particle voids [66]. The pore volume was greatest for CoP-LDH-3 at 0.42 $cm^3 \cdot g^{-1}$.

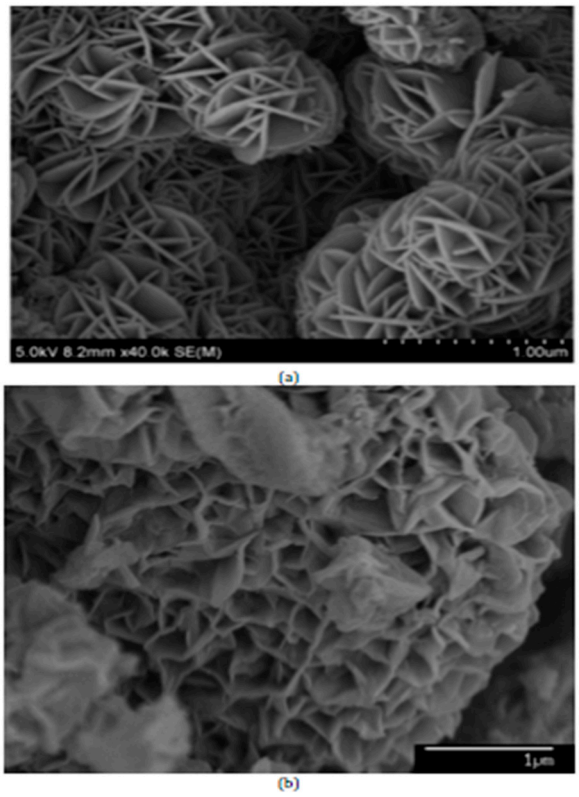

Figure 4. Scanning electron micrograph of prepared layered double hydroxide materials showing: (**a**) CoP-LDH-2; and (**b**) CoH-LDH-2.

Table 1. Powder X-ray diffraction, inductively coupled plasma spectroscopy, N_2 adsorption surface area analysis and qualitative surface basicity data (assessed use Hammett indicators) for prepared layered double hydroxide materials. Errors, where calculated, are shown in parentheses. The error in surface area determined by the N_2 adsorption method was estimated to be of the order of $\pm 5\ m^2 \cdot g^{-1}$.

Sample	a/Å	c/Å	Average Crystal Size a/nm	Average Crystal Size c/nm	PercentageAl %	Expected Ratio of Mg:Al	ICP Ratio of Mg:Al	Surface Area/$m^2 \cdot g^{-1}$	Pore Volume/$cm^3 \cdot g^{-1}$	Average Pore Size/nm	Surface Basicity/pH
CoP-LDH-2	3.05 (0.15)	22.94 (1.14)	255 (13)	221 (11)	31.9 (1.6)	2.0	1.7 (0.03)	91	0.32	9	9.0–10.0
CoP-LDH-3	3.06 (0.15)	23.42 (1.18)	198 (10)	129 (6)	25.1 (1.3)	3.0	2.7 (0.03)	82	0.42	14	7.6–9.0
CoP-LDH-4	3.07 (0.15)	23.65 (1.18)	254 (13)	133 (7)	20.2 (1.0)	4.0	3.3 (0.03)	17	0.12	21	9.0–10.0
CoP-LDH-5	3.08 (0.15)	23.83 (1.19)	168 (8)	114 (6)	18.3 (0.9)	5.0	4.0 (0.03)	24	0.17	20	9.0–10.0
CoP-LDH-6	3.08 (0.15)	23.82 (1.19)	161 (8)	91 (5)	18.0 (0.9)	6.0	5.2 (0.03)	39	0.25	22	9.0–10.0
CoH-LDH-2	3.14 (0.16)	23.50 (1.18)	312 (16)	140 (7)	-	2.0	1.3 (0.03)	33	0.05	10	6.0–7.6
CoH-LDH-3	3.14 (0.16)	23.93 (1.20)	301 (15)	102 (5)	-	3.0	2.3 (0.03)	42	0.08	10	6.0–7.6
CoH-LDH-4	3.14 (0.16)	24.26 (1.21)	289 (14)	138 (7)	-	4.0	3.7 (0.03)	46	0.10	11	6.0–7.6
CoH-LDH-5	3.14 (0.16)	23.98 (1.20)	387 (19)	116 (6)	-	5.0	3.2 (0.03)	42	0.09	13	7.6–9.0
CoH-LDH-6	3.14 (0.16)	23.86 (1.19)	337 (17)	189 (9)	-	6.0	5.0 (0.03)	43	0.10	11	7.6–9.0

2.1.2. Structure and Basicity of Mixed Metal Oxides Prepared from Co-Precipitated Layered Double Hydroxides

The PXRD patterns obtained for the CoP-MMOs are shown in Figure 3b and highlight the distinct structural changes that take place upon calcination of these LDH materials. The CoP-MMO structures show some evidence of rehydration for materials with *R*-values of 4 and 5, as nascent low angle peaks are observed. The reflections arising from the MMO materials are increasingly sharp as the *R*-value increases, indicating the presence of increased amounts of brucite in the original LDH materials [36]. Following calcination to the MMOs, a qualitative assessment of the surface basicity of these new materials was also undertaken using dry methanol solutions of Hammett basicity indicators (Table 2). This study showed that the basicities of the MMOs, CoP-MMO-1, CoP-MMO-3, CoP-MMO-4 and CoP-MMO-5, lie in the same range as those for their parent LDH materials. In contrast, the apparent basicity decreased for CoP-MMO-2 and CoP-MMO-6 to pH 7.6–9.0, relative to their corresponding LDH precursors.

Surface area analysis showed that for all LDH samples, their conversion to the corresponding MMO materials resulted in an increase in surface area, with a commensurate increase in total pore volume, but with a reduction in average pore volume/inter-particle voids (Table 2). The associated increase in surface area and pore volume is believed to occur due to fine pores forming perpendicular to the crystal surface during calcination, through which gases formed during the dehydroxylation process leave the crystal structure (i.e., water vapour and CO_2) [67–69].

Table 2. Surface area (N_2 adsorption) and qualitative surface basicity (assessed use Hammett indicators) data for prepared mixed metal oxides. The error in surface area determined by the N_2 adsorption method was estimated to be of the order of $\pm 5\ m^2 \cdot g^{-1}$.

Sample	Surface Area/$m^2 \cdot g^{-1}$	Pore Volume/$cm^3 \cdot g^{-1}$	Average Pore Size/nm	Surface Basicity (pH)
CoP-MMO-2	163	0.53	10	7.6–9.0
CoP-MMO-3	155	0.61	15	7.6–9.0
CoP-MMO-4	190	0.40	6	9.0–10.0
CoP-MMO-5	199	0.49	7	9.0–10.0
CoP-MMO-6	160	0.49	9	7.6–9.0
CoH-MMO-2	231	0.32	5	7.6–9.0
CoH-MMO-3	213	0.39	6	7.6–9.0
CoH-MMO-4	184	0.37	6	7.6–9.0
CoH-MMO-5	156	0.37	8	7.6–9.0
CoH-MMO-6	198	0.39	6	7.6–9.0

2.1.3. Structure and Basicity of Layered Double Hydroxides Prepared by Co-Hydration

The XRD data for the CoH-LDHs (Figure 3c) are characteristic of those from traditionally-prepared LDH materials, however it is clear that the new materials showed varying levels of impurity, as initially reported by Greenwell et al. [36], with significant quantities of brucite being detected for materials with *R*-values > 2. In addition, MgO phases are present in CoH-LDH-2 and CoH-LDH-4. As expected from LDHs containing adipate as the charge-balancing interlayer anion, PXRD analysis showed expanded phases (at 2-θ = 6°) for CoH-LDH-2 and CoH-LDH-3, where the adipate anion is perpendicular to the plane of the LDH sheet, and also the presence of collapsed phases (at 2-θ = 12°) for CoH-LDH-4 to CoH-LDH-6, where the adipate anion is parallel to the plane of the LDH sheet [59]. Unlike the CoP-LDHs, for the CoH-LDHs, the d_{110} LDH reflection was not distinct enough for correlation with the percentage of Al present in each LDH phase.

Thermogravimetric analysis of the CoH-LDH materials showed distinct mass losses associated with loss of water from intercalated water and layer hydroxyls, and carbon dioxide from interlayer adipate upon calcination to 500 °C (Supplementary materials). Expected and obtained Mg/Al ratios from ICP-OES for CoH-LDHs are shown in Table 1. The metal ion ratios determined by

ICP analysis generally increased with expected *R*-value, however CoH-LDH-5 (3.2) has a lower ratio than CoH-LDH-4 (3.7), something that has been attributed to the presence of impurities/heterogeneity.

Nitrogen adsorption/desorption experiments for CoH-LDHs all exhibited type IV isotherms characteristic of mesoporous materials [70]. In each case, the hysteresis loop was narrow, with almost parallel adsorption and desorption branches, something that is indicative of pores with regular geometry, while the steep desorption behaviour indicated that the pore size distribution was narrow (Sing et al., 1985) [70], centred at within 10–13 nm pore radius. The surface area for CoH-LDH-2 was 33 $m^2 \cdot g^{-1}$, considerably lower than that for the CoP-LDH-2 (91 $m^2 \cdot g^{-1}$). The surface areas of materials CoH-LDH-3 to CoH-LDH-6 are identical within error as a function of *R*-value (spanning values 42–46 $m^2 \cdot g^{-1}$) in contrast to the variation observed for their analogues prepared via co-precipitation. The average pore size was highest for CoH-LDH-5 (13 nm) and lowest for CoH-LDH-2 (9 nm and 10 nm, respectively).

A qualitative assessment of the surface basicity of each of the CoH-LDHs was determined (using the Hammett indicator method) and is shown in Table 1. The highest basicity was found for CoH-LDH-5 and CoH-LDH-6, lying in the range pH 7.6–9.0. The materials CoH-LDH-2 to CoH-LDH-4 were found to have estimated surface basicities lying in the range pH 6.0–7.6. Clearly, the basicity of the various CoP-LDH and CoH-LDH materials varies as a function of *R*-value, but also with the method used for their preparation. It is presumed this latter dependency arises as a consequence of differing morphologies that impact directly on the extents of surface edge/layer edges, which in turn alters the accessibility of surface basic sites.

2.1.4. Mixed Metal Oxides Prepared from Co-Hydration Layered Double Hydroxides

The PXRD data for the CoH-MMOs are shown in Figure 3d, and reveal that significant structural reorganisation takes place during the calcination process, with loss of the characteristic low angle basal LDH peaks in the PXRD patterns [71]. For each material, very sharp peaks were observed, something consistent with the presence of moderately crystalline MgO, although with some asymmetry, possibly due to an underlying partially substituted MgO-like material [59].

A qualitative assessment of the surface basicity for the CoH-MMOs is reported in Table 2. Following calcination, the basicity of the resulting MMOs has increased up to the pH 7.6–9.0 window, relative to the parent LDH, for the CoH-MMO-2 through to CoH-MMO-4 materials, but remained unchanged (pH 7.6–9.0) for CoH-MMO-5 and CoH-MMO-6. These results are distinct from those from the corresponding CoP-MMO materials, where at *R*-values of $\geq$4 no increase in surface basicity was observed. Post-calcination, increased surface basicity is generally attributed to the presence of remaining medium-strong Lewis basic O^{2-}–M^{n+} pairs along with strong basic sites relating to increased concentrations of O^{2-} species [31].

2.2. Analysis of Catalytic Ketonic Decarboxylation Reactions

Ketonic Decarboxylation of Stearic Acid

The catalytic performance of the as-prepared LDH and MMO materials was assessed for the ketonic decarboxylation of stearic acid, as described in Section 4.3 (250 °C, 17 bar, 24 h, dodecane solvent). Post-reaction, a soluble fraction and a wax-like fraction were both obtained in all cases. Initial analysis of the wax-like solid directly by $ASAP^+$ mass spectrometry identified the presence of stearone (18-pentatriacontanone), along with unreacted stearic acid (Figure 5). As a result, the waxy residues were rigorously extracted from the LDH/MMO catalyst under Soxhlet conditions using ethanol. The resulting organic phase was analysed using GC, as described in Section 4.4, and found to contain only unreacted acid and ketone product, in varying ratios (see Figure 6 for conversions of stearic acid to stearone). A control reaction with no LDH or MMO catalyst present was also run; no waxy material was observed to form under these conditions.

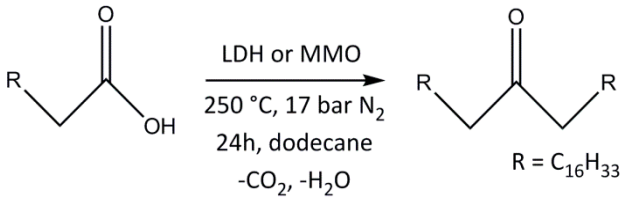

Figure 5. LDH-/MMO-mediated ketonic decarboxylation of stearic acid to stearone.

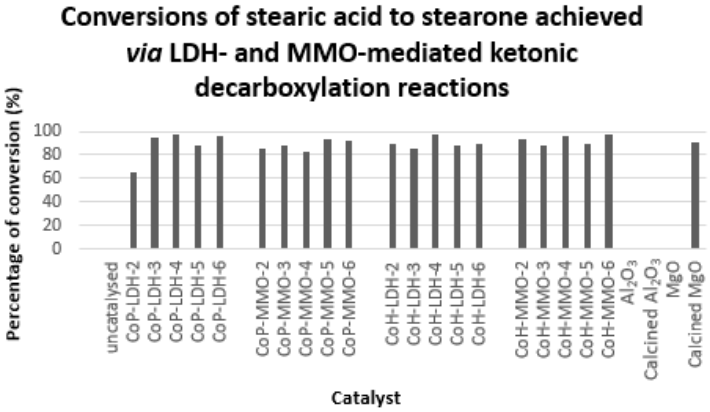

Figure 6. Conversions of stearic acid to stearone achieved via LDH- and MMO-mediated ketonic decarboxylation reactions, as well as the control reactions employed in this study (an analysis of error is presented in the supporting information). The Al_2O_3 was Catalyst Precursor (CP) grade. Reaction conditions: 250 °C, 17 bar N_2, 24 h, dodecane solvent; acid:catalyst ratio 5:1.

3. Discussion

3.1. Structure of Mixed Metal Oxide and Layered Double Hydroxide Catalysts

On the basis of the results from PXRD, TGA, and SEM analyses, all the CoH-LDH and CoP-LDH samples comprised typical LDH materials as the main phase. The co-hydrated adipate LDH samples showed similar structures to those reported previously by Greenwell et al. [36], while the co-precipitated samples showed characteristic structures for similarly-prepared materials reported in the literature [32]. For all of the LDH materials synthesised here, calcination resulted in loss of the typical layered LDH structure, affording a low order mixed-metal oxide phase. Nitrogen adsorption/desorption isotherms indicated that narrower pore size distributions were achieved using the co-hydration method, with CoH-LDHs exhibiting very narrow hysteresis with similar pore size distributions. The surface areas and pore volumes of the various materials increased greatly on calcining from LDH to MMO, with all surface areas being greater than 153 $m^2 \cdot g^{-1}$. The average pore diameters were found to increase for CoP-MMO-1 to CoP-MMO-3, however CoP-MMO-4 to CoP-MMO-6 and all CoH-MMO samples were found to decrease in pore volume compared to their LDH precursors, although their pore dimensions remained in the mesoporous range. During the calcination step, loss of water and interlayer anions was found to occur, as shown by TGA–mass spectrometry, confirming the transition from LDHs to MMOs (see Figure S1).

3.2. Ketonic Decarboxylation Reactions

The reaction showed good conversion of stearic acid to stearone via ketonic decarboxylation in the presence of each of the mixed-metal (both MMO and LDH) materials prepared. No other products were observed via GC analyses of the soluble reaction products or by ASAP-MS analysis of the waxy solid materials consistent with complete selectivity towards the ketone.

To understand the reactivity of the different catalysts, a range of structural and chemical characterisation methods were applied to the materials used. MMOs have unique structural differences

relative to LDHs that can be observed with PXRD. The PXRD analysis of the MMO materials generated from LDHs synthesised via co-hydration (CoH-MMOs) were noted to contain crystalline MgO co-phases, although these were not observed to impact on the degree of conversion of stearic acid. The CoP-MMOs with broader (FWHM) MgO peaks, indicating less ordered crystal structure and smaller particle size, are equally as active (within experimental error) as the CoH-MMOs, for the catalysis of stearic acid to stearone showing the presence of impurity in the more environmentally friendly CoH material preparation does not adversely impact reactivity (See Figure 7).

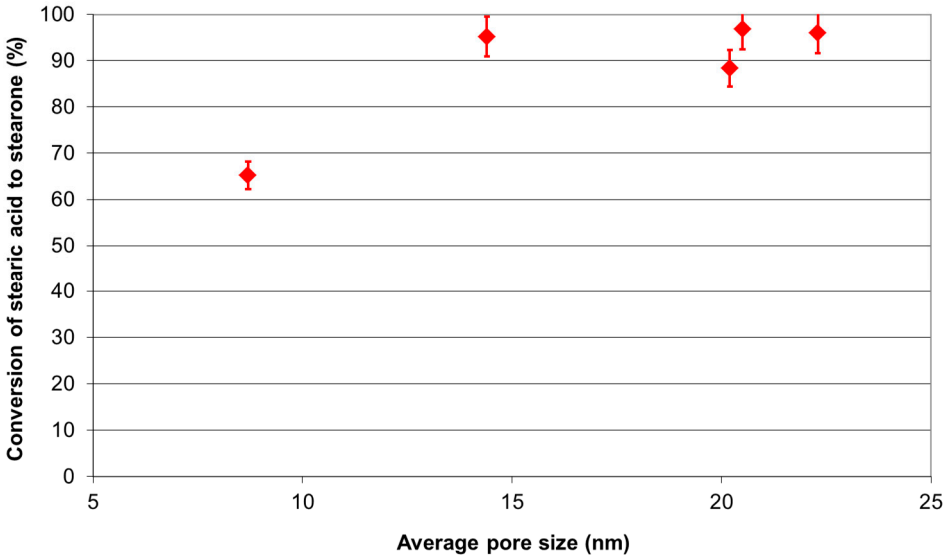

Figure 7. Conversion of stearic acid to stearone vs. average pore size for the oxide materials CoP-LDH-2 to CoP-LDH-6. Where pore sizes of 9, 14, 21, 20 and 22 nm correspond to CoP-LDH-2, CoP-LDH-2, CoP-LDH-2, CoP-LDH-2 and CoP-LDH-2, respectively.

Since control reactions using stearic acid undertaken with identical reaction conditions, but in the absence of catalyst, showed no ketone product, thermal activation pathways for the formation of stearone have been ruled out. It is therefore proposed that one of the roles of the LDH/MMO mineral catalyst used within this study is to organise the reactant stearic acid molecules favourably at its surface, as proposed computationally by Ignatchenko [22]. Assuming that in the mineral surface-mediated ketonic decarboxylation reaction the product reflects the original reactant carboxylic acid molecule alignment, a head-to-head arrangement would be favourable for ketonic decarboxylation. Indeed, previously, the organisation of carboxylate groups at LDH surfaces has been shown to control the outcome of photochemical cycloaddition reactions of both cinnamate [72,73] and stilbene carboxylates [74]. Moreover, other studies using transition metal oxides have also shown the role of surface promotion in ketonic decarboxylation [23], as well as in decarboxylation [75]. Ketonic decarboxylation has previously been shown to involve Lewis acid and Brønsted basic sites on metal oxides [19], with a possible similar mechanism occurring here involving base site abstraction of an α-proton and formation of a β-keto acid intermediate.

To further probe the LDH-/MMO-mediated ketonic decarboxylation of stearic acid, an alternative reaction was undertaken using CP5 Al_2O_3 as the catalyst under identical process conditions (Figure 6). In the presence of both calcined and as-received CP5 Al_2O_3, no reactivity was observed after 24 h. This suggests that ketonic decarboxylation requires more than just physisorption at a mineral surface for substrate pre-organisation, with the chemical nature of the surface also playing a controlling factor. Acidic/neutral Al_2O_3 was not found to promote ketonic decarboxylation under the reaction conditions employed herein, suggesting the reaction occurs through basic sites and proton abstraction, consistent with previous studies (vide supra).

In the conversion of stearic acid via ketonic decarboxylation to stearone, all the LDHs and MMOs prepared here exhibited sufficient base catalytic sites, with no discernible differences between them. Consequently, in order to probe stearone formation in greater detail, reactions of stearic acid were undertaken with calcined and as received MgO as a catalyst. As-received MgO resulted in 0.5% conversion of stearic acid to stearone (at 250 °C), whereas MgO calcined at 500 °C led to 90.0% conversion. This latter observation is consistent with a previous report that demonstrated ketonic decarboxylation of lauric acid catalysed by solid MgO, but at much higher reaction temperatures (>400 °C) than those we report here [76]. Previous studies of the calcination of MgO have shown that basic, non-hydrogen-bonded surface OH groups are formed at the surface of the MgO [77]. In the context of the current study, it is interesting that MgO is activated by calcination, leading to a higher conversion of stearic acid to stearone relative to that achieved with the uncalcined precursor. It might be expected that the MMOs with high Mg content would behave more akin to the MgO phase, which, as discussed, is known to be active in these reactions. Thus, in this present study, the conversion of stearic acid to stearone by MgO may be attributed to reaction occurring at weakly basic OH groups on the oxides' surface. In summary, these results show that a mineral surface containing basic active sites is needed for efficient decarboxylation, again consistent with previous metal oxide-mediated ketonisation reactions.

Direct decarboxylation of stearic acid to *n*-heptadecane in dodecane solution was not found to occur, with any of the catalysts employed in this present study for reactions undertaken at 250 °C. This lack of direct decarboxylation is in agreement with a previous study by Na et al. who found that, with similar mixed metal oxides to those employed here, full decarboxylation of oleic acid only occurred at temperatures above 350 °C [78]. This prior study also reported minimal acid conversion was achieved below 350 °C, and that the formation of a waxy solid substance occurred, which the authors attributed to formation of a Mg-oleate saponification product. However, in our study this waxy material has unequivocally been identified as stearone.

From our studies of various different CoP-LDH catalysts it can be seen that there is a relationship between average pore size and conversion of stearic acid to stearone (Figure 7). Converting two molecules of stearic acid, with an 18-carbon backbone chain, into stearone, with a 35-carbon backbone chain may be sterically hindered with the catalysts that exhibit small pore size. The data presented in Figure 6 show that, for CoP-LDH-2 to CoP-LDH-6, conversion to stearone was between 88% and 97%, for pore sizes of 14 nm and above, suggesting there is a lowest optimum pore size for this reaction. With the reaction converting two long chain fatty acid molecules into similarly long chain ketone product molecules, accessibility to catalytic sites may be sterically hindered by the small average pore size of CoP-LDH-2 (9 nm). Similar trends were not observed for tests carried out using the materials CoH-LDHs, CoP-MMOs or CoH-MMOs.

Other authors have also studied ketonic decarboxylation with heterogeneous base catalysts. For example, although Das and Parida found that using a ZnAl-MMO material with *R*-value 3 led to a good yield of acetone (>89%) from acetic acid, a much higher reaction temperature of 425 °C was required compared to that employed in our study, 250 °C [47]. The ZnAl-MMO material used by Das and Parida had a lower surface area (103.5 $m^2 \cdot g^{-1}$) even compared to the smallest surface area measured for the CoP-MMOs used here (155 $m^2 \cdot g^{-1}$ for CoP-MMO-3)—something that could contribute to the lower reactivity of the ZnAl-based material.

Other oxides such as ceria have also been used as catalysts in ketonic decarboxylation reactions. For example, Nagashima et al. found that use of a CeO_2-Mn_2O_3 material led to 73.9% conversion of propanoic acid to propanone with 97.4% selectivity at 350 °C, whereas CeO_2-MgO had a lower (66.8%) conversion, but with similarly high selectivity [12]. The authors speculated the reaction mechanism involved adsorption of carboxylates, followed by abstraction of an α-proton to create a radical, which formed a β-keto acid with a second carboxylate, followed by decarboxylation to the ketone. When using mixed acid feedstocks with ceria-zirconia catalysts, the cross-ketonic decarboxylation

was found to proceed at a faster rate than homo-ketonic decarboxylation [79]. However, such a redox driven process is not feasible in the MgAl systems employed in the current study.

3.3. Comparison of Ketonic Decarboxylation by Mixed Metal Oxides versus Layered Double Hydroxides

In the study presented here, all MMO and LDH materials brought about the same degree of stearic acid conversion to stearone within error (Figure 6). This suggests that in this transformation the MMO and LDH catalysts are of similar reactivity, something supported qualitatively by the qualitative Hammett indicator-based assessment of basicity (vide supra). Furthermore, since during ketonic decarboxylation, water and carbon dioxide are both lost from the reacting carboxylic acid molecules, it may be reasonable to suggest that this may lead to partial reconstruction of the MMO materials back to LDH-like systems (a well-established phenomenon [49]), something that is likely to be most prevalent at the surfaces of the oxides rendering the materials essentially identical. Conversely, at a reaction temperature of 250 °C, TGA analysis clearly identified that the LDH catalysts undergo partial dehydroxylation to form MMO phases. As such, under the test conditions employed in the ketonisation reactions described herein, the reactive surfaces of the LDH and corresponding MMO materials are likely to have similar structure and reactivity, though it is notable that the increased surface area of the MMO materials over the LDHs does not seem to have an effect on performance. At present, no attempt has been made within this initial study to assess the reaction kinetics, and it is possible that the 24 h reaction period results in equilibrium being reached for both sets of catalyst. Work is ongoing to investigate the effect of both reaction time and temperature.

3.4. Comparison of Ketonic Decarboxylation by Co-hydrated and Co-precipitated Catalysts as a Function of Mg/Al Ratio

For those catalyst materials with an *R*-value of 2, CoP-LDH-2 was found to catalyse the reaction with a relatively low yield of stearone (65.2%) relative to that observed for CoH-LDH-2, 89.5%. Out of the catalysts tested, CoH-MMO-2 exhibited the greatest conversion 93.6%, and showed a slightly (within error) increased reactivity compared to that achieved using CoP-MMO-2 (85.9%). In contrast, for catalysts with an *R*-value of 3, the highest conversion was with CoP-LDH-3 (95.2%), followed by CoH-MMO-3 and then CoP-MMO-3. For an *R*-value of 4, CoH-LDH-4 had greatest reactivity (97.1% stearone), followed by CoP-LDH-4 and CoH-MMO-4. For $R = 5$ and $R = 6$ the greatest conversions were with the CoP-MMOs and CoH-MMOs, respectively. The materials CoH-MMO-6 (97.2%), CoH-LDH-4 (97.1%), CoP-LDH-6 (96.8%), CoP-LDH-6 (96%) and CoH-MMO-4 (95.4%) all gave conversions identical within error.

The similarity in catalytic performance determined across the materials makes it somewhat difficult to draw firm conclusions on the effect of preparation method. In part, this is due to variability in the extraction and purification processes. In essence, it may be stated that all LDH/MMO catalysts prepared exhibit similar performance for ketonic decarboxylation. Through examining the effect of reaction time/temperature, further work will seek to determine differences between the catalysts on the basis of reaction kinetics.

4. Materials and Methods

All chemicals and reagents were used as received from commercial sources, without further purification: magnesium nitrate hexahydrate (ACS grade, 99%), sodium bicarbonate (ACS grade, 99.7%), magnesium oxide (ACS grade, 98%), adipic acid (99%), dodecane (98%), and aluminium nitrate nonahydrate (ACS grade, 98%) were obtained from Sigma Aldrich (Sigma-Aldrich Company Ltd., Dorset, UK); NaOH (AR grade) was purchased from Fisher Scientific UK (Loughborough, UK); activated aluminium oxide (CP5) was kindly supplied by BASF (Hannover, Germany); stearone (95%) from TCI (Oxford, UK); and *n*-heptadecane (99%), stearic acid (97%), pyridine (analytical grade), *N*,*O*-*bis*(trimethylsilyl)trifluoroacetamide (BSTFA) (98+% and eicosane (99%) from Acros

Organics (Loughborough, UK). A C_8-C_{20} alkane GC standard solution was purchased from Fluka (Loughborough, UK).

4.1. Sample Nomenclature

The catalyst samples are described according to: (i) the method of preparation, CoP = co-precipitation and CoH = co-hydration; (ii) whether LDH or MMO; and (iii) the starting Mg/Al stoichiometry or *R*-value.

4.2. Catalyst Preparation

4.2.1. Preparation of Layered Double Hydroxides by Co-Precipitation

The carbonate LDHs, CoP-LDH-2–CoP-LDH-6 were prepared using a co-precipitation method. A typical preparation is outlined here for CoP-LDH-2, with the quantities used in each of the other preparations given in the Supplementary Materials (Table S1). A solution (100 mL) containing magnesium nitrate hexahydrate (2.312 g, 9.000 mmol) and aluminium nitrate nonahydrate (1.688 g, 4.500 mmol) was added drop-wise into continuously stirred solution of sodium bicarbonate (3.770 g 44.877 mmol) in water (100 mL) held at 65 °C. A constant pH (pH 10) was maintained by the simultaneous addition of an aqueous solution of 1M NaOH. After complete addition of the $Mg(NO_3)_2/Al(NO_3)_3$ solution, the ensuing reaction mixture was aged at 65 °C for 5 h and filtered. The resulting white solid was washed with hot deionised water (1 L) to remove any remaining Na^+ ions, and then dried overnight in an oven at 80 °C under air.

4.2.2. Preparation of Layered Double Hydroxides via Co-Hydration

LDHs CoH-LDH-2–CoH-LDH-6 were prepared using a co-hydration method as developed by Greenwell et al. [36] which allows the synthesis of Na^+-free, high aspect ratio LDHs, without the need for an inert atmosphere. A representative procedure describing the preparation of CoH-LDH-2 is as follows. CP5 aluminium oxide (1.01 g, 19.8 mmol) was added to water (100 mL), with continuous stirring, at 65 °C. After 10 min adipic acid (AA) was added as a peptising agent (0.6 AA:Al; 11.900 mmol, 1.737 g). After a period of 50 min, solid magnesium oxide (1.49 g, 37.0 mmol) was added to the mix, to give a 1% slurry based on total oxide content. The ensuing reaction mixture was aged at 65 °C for 5 h to afford a white precipitate, which was isolated by filtration and dried overnight in an oven at 80 °C under air. The stoichiometry of the reagents used is given in Table S2.

4.2.3. Mixed Metal Oxide Preparation

The MMO materials (CoH-MMO and CoP-MMO) were prepared immediately prior to use by calcination of the corresponding LDH loose powder in a horizontal crucible at 500 °C under air for 3 h in a quartz tube open at each end. The resulting samples were quickly and carefully transferred from the furnace at 500 °C and placed in a desiccator under vacuum to cool before being weighed and placed in the reaction vessel.

4.3. Material Characterisation

4.3.1. Powder X-ray Diffraction

Solid materials were analysed by powder X-ray diffraction (PXRD) using a Philips X'pert PW3710 diffractometer (Malvern Panalytcial, Worcestershire, UK) with Cu Kα radiation (λ = 1.5418 Å) and scanned in the range 2θ = 3–80° under ambient atmospheric conditions. LDHs were analysed following drying at 80 °C, while MMOs were analysed immediately on cooling to room temperature under vacuum. All samples were manipulated under ambient atmospheric conditions, ground to a fine powder and mounted on thin glass slide sample holders.

4.3.2. Thermal Analysis

Thermogravimetric analyses (TGA) were undertaken using a Perkin Elmer Pyris 1 instrument (Perkin Elmer, Sear Green, UK). Samples were heated from room temperature to 1000 °C under a nitrogen atmosphere at flow rate of 20 mL/min and a heating rate of 10 °C/min and cooled back to room temperature at a rate of 10 °C/min. Mass changes for the various LDH materials were monitored on heating from room temperature to 500 °C and upon subsequent cooling back to room temperature both at a rate of 10 °C/min. Coupled TGA-mass spectrometry was used to study the evolution of CO_2 (from pyrolysis of the adipate anions) and of H_2O, both as a function of temperature.

4.3.3. Scanning Electron Microscopy (SEM)

A cotton bud was used to sprinkle the sample of finely ground LDH or MMO onto a carbon pad mounted on an aluminium stub. The sample was then coated with 15 nm thick layer of Pt using a Cressington 328 UHR Sputtering system. A Hitachi SU70 analytical Scanning Electron Microscope (SEM) (Hitachi High Technologies, Krefeld, Germany) was then used to produce images of the surface of the various materials employing an accelerating voltage of 5 kV under a vacuum of 3 mbar.

4.3.4. Inductively Coupled Plasma Optical Emission Spectroscopy

Materials were analysed using a Perkin Elmer Optima 3300RL instrument (Perkin Elmer, Sear Green, UK), which was calibrated with Mg/Al standards (2 ppm, 5 ppm, 10 ppm) made from Romil 1000 ppm stock solutions. Multiple wavelengths (aluminium: 396.193 nm, 308.215 nm, 394.401 nm, and 237.313 nm; and magnesium: 285.213 nm, 279.077 nm, 280.271 nm, and 279.552 nm) were measured to confirm these were interference-/error-free. Standard solutions were analysed every 10 samples to reconfirm instrument calibration.

4.3.5. Surface Area Analysis

Specific surface area, pore volume, and average pore size measurements were performed using an N_2 adsorption and desorption method at −196 °C using a Micromeritics ASAP 2020 system (Micromeritics, Hexton, UK). For each sample analysed, 0.5 g of finely ground sample was placed in a pre-weighed analysis tube which was connected with a de-gas port and heated at 80 °C (LDH) or 200 °C (MMO) for 4 h under a vacuum of 200 μm Hg to remove any volatile materials adsorbed on the surface. After this, the sample was cooled to room temperature and then the tube with degassed sample was re-weighed. An isothermal jacket was placed over the tube and it was connected to an analysis port, cooled under liquid N_2 and degassed. The sample then underwent nitrogen adsorption/desorption at various pressures. The density of the samples, required for pore size analysis, was determined using an AccuPyc II 1340 Pycnometer (Micromeritics Instrument Corp., Norcross, GA, USA). The error in surface area determined by the N_2 adsorption method was estimated to be of the order of 5 $m^2 \cdot g^{-1}$.

4.3.6. Estimation of basicity

Attempts were made to estimate qualitatively the basicity of the various solid materials using methods previously described in the literature [31,45]. Thus, qualitative basicity determinations were attempted using dry methanol solutions of the appropriate Hammett base indicators bromothymol blue (pH range 6.0–7.6), *m*-cresol purple (pH range 7.6–9.2), phenolphthalein (pH range 8.0–10.0) and indigo carmine (pH range 11.5–13.0). The methanol-indicator solutions were added to the solid LDH/MMO samples until there were no further colour changes associated with increasing basicity. Attempts to further quantify basicity were made using FTIR spectroscopy of surface bound pyrrole probe molecules (see Figures S7 and S8) on two of the samples, however the data gave little extra insight than the Hammett indicators and further samples were not run. FTIR spectra were collected using a Thermo iS10 spectrometer (Waltham, MA, USA) equipped with a DTGS detector in the range 6000–1000 cm^{-1} with the resolution of 4cm^{-1} and 64 scans in transmission mode. Prior to recording

the spectra, the self-supported sample disks (~10 mg/cm^2) were heated in a vacuum cell at 30–450 °C (ramp 1°C/min). After a period of 5 h at the selected temperature, the sample was cooled to 30 °C in vacuum and its IR spectrum was collected.

4.4. Stearic Acid Ketonic Decarboxylation Studies

A stirred 100 mL Parr autoclave was charged with stearic acid (0.1 g, 0.35 mmol), dodecane (10 mL) as solvent, and 20 wt % LDH or MMO (0.02 g) and subsequently purged with nitrogen. The vessel was then pressurised using nitrogen gas to 17 bar to allow comparison with a prior study [80], and heated to achieve a final temperature (internal) of 250 °C and the reaction then stirred for a period of 24 h. The vessel was then allowed to cool and the reaction mixture, containing the solid oxide and wax residues, filtered through a sintered glass frit. The filtrate was retained for analysis (described below) and the solid/wax fraction subjected to Soxhlet extraction using ethanol (250 mL) at reflux for a period of 12 h to remove any reactants or wax products from the oxide materials. The resulting ethanolic fraction was analysed as described in the next section.

4.5. Product Analysis

Prior to separation by Soxhlet extraction, waxy solids, observed intermingled with the catalyst, were analysed using a Xevo QToF mass spectrometer (Waters Ltd., Hertfordshire, UK) equipped with an Agilent 7890 GC (Agilent Technologies UK Ltd., Stockport, UK) and an atmospheric solids analysis probe (ASAP) solid handling sample introduction port. Solid samples were introduced into the spectrometer from a heated glass melting point tube (ramp from 100 to 600 °C over several minutes) previously dipped into neat sample. Mass spectrometry data were processed using MassLynx 4.1 (Waters Inc, Milford, MA, USA). Exact mass measurements were recorded using a lock-mass correction to provide <3 mDa precision.

The wax products were also analysed quantitatively, after Soxhlet extraction (to remove any residual Mg/Al oxide/hydroxide) as ethanol solutions, using gas chromatography (HP 5890—Series 2) with a TR-SD capillary column (length 10 m, ID 0.53 mm and film thickness 2.65 μm) with retention times corroborated using standard materials. Data analysis and peak integration were performed using Clarity software (DataApex, Prague, Czech Republic, 2003). The liquid phase of the reaction was also analysed by the HP 5890 Series II GC-FID (Agilent Technologies, Santa Clara, CA, USA), with a representative trace shown in Figure S2. Calibration curves of the mixtures were prepared according to Table S3 and the analysis of these are shown in Figure S3.

To validate the efficiency of the Soxhlet extraction process and analysis, a range of standard concentrations of stearic acid-stearone mixtures (Tables S4 and S5) were extracted and compared to the actual stearic acid-stearone concentrations obtained from the ethanolic solutions (see above paragraph), by GC, with the data shown in Figures S4 and S5. It was found that the validation curves showed higher significance for stearone than for stearic acid, and so these were used for reaction conversion values.

5. Conclusions

Essentially independent of their composition (*R*-values = 1–6) and method of preparation, cheap, non-toxic, Al/Mg LDHs and MMOs all mediate the ketonic decarboxylation of stearic acid to stearone at moderate temperatures (250 °C) with excellent conversion (~90%). The identical behaviour of each of these mixed metal oxide materials, which only vary slightly in both their surface basicity and structure, indicated that the decarboxylation of the carboxylic acid occurs on the oxides' surfaces. In part, this is likely to result from the ability of the charged mineral surface to align the carboxylic acids in a preferred head-to-head configuration, as has been suggested from previous computational studies [23]. Little difference in reactivity towards stearic acid was observed between LDH materials prepared by either co-hydration or co-precipitation, indicating contamination from NaOH entrained during synthesis was not responsible for the reactivity (none was added to the co-hydrated materials),

and even between LDH and their corresponding MMO counterparts. The similarity in performance of the LDH and MMO materials further suggested that under the reaction conditions the possibility of partial conversion of the LDH materials towards their sibling MMO materials occurring under reaction conditions (onset of LDH dehydroxylation established to commence at 250 °C), and/or by in situ rehydration of MMO materials back towards LDH-type systems caused by water generated during reaction are likely. Consequently, for this ketonic dehydroxylation, the more environmentally preferable co-precipitation clay synthesis is preferable [36], avoiding the production of highly basic supernatants. The requirement of costly and energetic catalytic activation procedures can be eliminated with the LDHs showing comparable efficacy in catalysis as their corresponding MMOs (prepared from the LDHs by calcination), over the 24 h reaction and under batch conditions, enhancing the green principles of the process [81]. Interestingly, although the initial LDHs prepared by co-hydration were not phase pure by PXRD, the $Mg(OH)_2$ impurities did not adversely affect the catalytic reaction. The values of stearone yield reported use the figures obtained from the stearone calibration curve, whereas the extraction process incorporates further error onto this evaluation, so the performance of all the active CoH-LDHs and CoH-MMOs are assumed to be the same within this error.

In summary, Mg/Al MMO and LDH materials were efficient catalysts for promoting ketonic decarboxylation of stearic acid and offer promise in algal biomass lipid fraction upgrading reactions. Work is presently underway to optimise the reaction conditions in terms of pressure and time. Future studies will explore the effect of carboxylic acid chain length and also reaction temperature will be studied to determine the transition between decarboxylation and ketonic decarboxylation reaction mechanisms. Ketonic decarboxylation holds promise to efficiently provide an alternative, non-petroleum route to ketones, directly from plant and algal oils and without the need of oxidation chemistry.

Supplementary Materials: The following are available online at http://www.mdpi.com/2304-6740/6/4/121/s1, Figure S1: Thermogravimetric analyses of co-hydrated LDH (CoH-LDH) catalyst materials with different Mg/Al ratios, Figure S2: A typical GC chromatogram for silylated stearic acid (~33.0 min) and *n*-heptadecane (~6.6 min) with the internal standard eicosane (~14.8 min) in the solvent dodecane (~2min), Figure S3: Calibration curves obtained by gas chromatography for (a) silylated stearic acid and (b) *n*-heptadecane in dodecane, Figure S4: Calibration curve obtained by GC for silylated stearic acid analysed as a THF solution, Figure S5: Calibration curve obtained for Stearone based on dilution factors of the stock solution SeE, Figure S6: FTIR spectra of pyrrole adsorbed on ion-exchanged faujasites, Figures S7 and S8: FTIR spectra of pyrrole adsorbed on CoH-MMO-3 and CoP-MMO-3. Tables S1 and S2: Masses, moles and ratios of the reactants used for each R-value LDH co-precipitation and LDH co-hydration preparation, Table S3: Reference samples prepared for calibration of stearic acid, and *n*-heptadecane, Table S4: Reference samples prepared for calibration of stearic acid in THF, Table S5: Dilutions of the stock solution SeE used in stearone GC calibration, Table S6: Pyrrole adsorption on FAU type zeolites and LDH catalysts. References [82–86] are cited in the supplementary materials.

Author Contributions: Conceptualization, H.C.G. and B.S.; methodology, H.C.G., B.S.; formal analysis, B.S., L.L. and L.F.G.; FTIR characterisation of the acid–base properties of the investigated materials, V.L.Z; investigation, B.S., L.L. and L.F.G.; writing—original draft preparation, B.S., H.C.G. and P.W.D.; writing—review and editing, L.L., L.F.G., D.D.P.-S., H.C.G. and P.W.D.; supervision, H.C.G. and P.W.D.; and funding acquisition, H.C.G. and P.W.D.

Funding: This research was funded by EPSRC and KiOR Inc. via a CASE Studentship (B.S.) and through the EU FP7 programme "BioAlgaeSorb" (L.L., H.C.G. and P.W.D.). D.P.-S. acknowledges CoNACYT for a PhD studentship. L.F.G. was funded through an EPSRC Impact Accelerator Award.

Acknowledgments: We thank Leon Bowen, Department of Physics, Durham University for assistance with electron microscopy used in this study. We also acknowledge Pieter Bruijnincx at Utrecht University for extremely helpful feedback and comments on an earlier version of this manuscript.

Conflicts of Interest: The authors declare no conflict of interest.

References

1. Demirbas, A. Political, Economic and Environmental Impacts of Biofuels: A Review. *Appl. Energy* **2009**, *86*, S108–S117. [CrossRef]
2. Roddy, D.J. Biomass in a Petrochemical World. *Interface Focus* **2013**, *3*, 20120038. [CrossRef] [PubMed]
3. Speight, J. *The Biofuels Handbook*; RSC Publishing: London, UK, 2011.

4. McNeil, J.; Day, P.; Sirovski, F. Glycerine from Biodiesel: The Perfect Diesel Fuel. *Process Saf. Environ. Prot.* **2012**, *90*, 180–188. [CrossRef]
5. Carlos Serrano-Ruiz, J.; Pineda, A.; Mariana Balu, A.; Luque, R.; Manuel Campelo, J.; Angel Romero, A.; Manuel Ramos-Fernandez, J. Catalytic transformations of biomass-derived acids into advanced biofuels. *Catal. Today* **2012**, *195*, 162–168. [CrossRef]
6. Shylesh, S.; Gokhale, A.; Ho, C.; Bell, A. Novel Strategies for the Production of Fuels, Lubricants, and Chemicals from Biomass. *Acc. Chem. Res.* **2017**, *50*, 2589–2597. [CrossRef] [PubMed]
7. Rattanasumrit, A.; Ruangpornvisuti, V. Theoretical Study of Conversion Reactions of Ketone to Hydroxyalkylene in Cluster Models of Zeolite H-ZSM-5. *J. Mol. Catal. A Chem.* **2005**, *239*, 68–75. [CrossRef]
8. Guo, Z.; Wang, S.; Zhu, Y.; Li, X.; Luo, Z. Catalytic Cracking of Ketone Components in Biomass Pyrolysis Oil. In Proceedings of the 2010 Asia-Pacific Power and Energy Engineering Conference (APPEEC), Chengdu, China, 28–31 March 2010; pp. 1–3.
9. Snell, R.W.; Shanks, B.H. Insights into the Ceria-Catalyzed Ketonization Reaction for Biofuels Applications. *ACS Catal.* **2013**, *3*, 783–789. [CrossRef]
10. Siegel, H.; Manfred, E. Ketones. In *Ullmann's Encyclopedia of Industrial Chemistry*; John Wiley & Sons: Hoboken, NJ, USA, 2000.
11. Deng, L.; Fu, Y.; Guo, Q.-X. Upgraded Acidic Components of Bio-oil through Catalytic Ketonic Condensation. *Energy Fuels* **2009**, *23*, 564–568. [CrossRef]
12. Nagashima, O.; Sato, S.; Takahashi, R.; Sodesawa, T. Ketonization of carboxylic acids over CeO_2-based composite oxides. *J. Mol. Catal. A Chem.* **2005**, *227*, 231–239. [CrossRef]
13. Shutilov, A.A.; Simonov, M.N.; Zaytseva, Y.A. Phase composition and catalytic properties of ZrO_2 and CeO_2-ZrO_2 in the ketonization of pentanoic acid to 5-nonanone. *Kinetics Catal.* **2013**, *54*, 184–192. [CrossRef]
14. Gaertner, C.A.; Serrano-Ruiz, J.C.; Braden, D.J.; Dumesic, J.A. Catalytic Coupling of Carboxylic Acids by Ketonization as a Processing Step in Biomass Conversion. *J. Catal.* **2009**, *266*, 71–78. [CrossRef]
15. Yamada, Y.; Segawa, M.; Sato, F.; Kojima, T.; Sato, S. Catalytic Performance of Rare Earth Oxides in Ketonization of Acetic Acid. *J. Mol. Catal. A Chem.* **2011**, *346*, 79–86. [CrossRef]
16. Jackson, M.A.; Cermak, S.C. Cross Ketonization of *Cuphea sp* Oil with Acetic Acid over a Composite Oxide of Fe, Ce, and Al. *Appl. Catal. A Gen.* **2012**, *431*, 157–163. [CrossRef]
17. Pestman, R.; Koster, R.M.; van Duijne, A.; Pieterse, J.A.Z.; Ponec, V. Reactions of Carboxylic Acids on Oxides: 2. Bimolecular Reaction of Aliphatic Acids to Ketones. *J. Catal.* **1997**, *168*, 265–272. [CrossRef]
18. Corma, A.; Borja, O.T.; Renz, M.; Simakova, I.L. Conversion of levulinic acid derived valeric acid into a liquid transportation fuel of the kerosene type. *J. Mol. Catal. A Chem.* **2014**, *388–389* (Suppl. C), 116–122. [CrossRef]
19. Pham, T.N.; Sooknoi, T.; Crossley, S.P.; Resasco, D.E. Ketonization of Carboxylic Acids: Mechanisms, Catalysts, and Implications for Biomass Conversion. *ACS Catal.* **2013**, *3*, 2456–2473. [CrossRef]
20. Pacchioni, G. Ketonization of Carboxylic Acids in Biomass Conversion over TiO_2 and ZrO_2 Surfaces: A DFT Perspective. *ACS Catal.* **2014**, *4*, 2874–2888. [CrossRef]
21. Neunhoeffer, O.; Paschke, P. Über den Mechanismus der Ketonbildung aus Carbonsäuren. *Berichte der deutschen chemischen Gesellschaft* **1939**, *72*, 919–929. [CrossRef]
22. Ignatchenko, A.V. Density Functional Theory Study of Carboxylic Acids Adsorption and Enolization on Monoclinic Zirconia Surfaces. *J. Phys. Chem. C* **2011**, *115*, 16012–16018. [CrossRef]
23. Ignatchenko, A.V.; Kozliak, E.I. Distinguishing Enolic and Carbonyl Components in the Mechanism of Carboxylic Acid Ketonization on Monoclinic Zirconia. *ACS Catal.* **2012**, *2*, 1555–1562. [CrossRef]
24. Randery, S.D.; Warren, J.S.; Dooley, K.M. Cerium Oxide-based Catalysts for Production of Ketones by Acid Condensation. *Appl. Catal. A Gen.* **2002**, *226*, 265–280. [CrossRef]
25. Pham, T.N.; Shi, D.; Resasco, D.E. Kinetics and Mechanism of Ketonization of Acetic Acid on Ru/TiO_2 Catalyst. *Top. Catal.* **2014**, *57*, 706–714. [CrossRef]
26. Pulido, A.; Oliver-Tomas, B.; Renz, M.; Boronat, M.; Corma, A. Ketonic Decarboxylation Reaction Mechanism: A Combined Experimental and DFT Study. *ChemSusChem* **2013**, *6*, 141–151. [CrossRef] [PubMed]
27. Kumar, R.; Enjamuri, N.; Shah, S.; Sadeq Al-Fatesh, A.; Bravo-Suárez, J.J.; Chowdhury, B. Ketonization of Oxygenated Hydrocarbons on Metal Cxide based Catalysts. *Catal. Today* **2018**, *302*, 16–49. [CrossRef]
28. Evans, D.G.; Slade, R.C.T. Structural Aspects of Layered Double Hydroxides. *Struct. Bond.* **2006**, *119*, 1–87.

29. Wang, Q.; O'Hare, D. Recent Advances in the Synthesis and Application of Layered Double Hydroxide (LDH) Nanosheets. *Chem. Rev.* **2012**, *112*, 4124–4155. [CrossRef] [PubMed]
30. Cavani, F.; Trifirò, F.; Vaccari, A. Hydrotalcite-type Anionic Clays: Preparation, Properties and Applications. *Catal. Today* **1991**, *11*, 173–301. [CrossRef]
31. Debecker, D.P.; Gaigneaux, E.M.; Busca, G. Exploring, Tuning, and Exploiting the Basicity of Hydrotalcites for Applications in Heterogeneous Catalysis. *Chem. A Eur. J.* **2009**, *15*, 3920–3935. [CrossRef] [PubMed]
32. Miyata, S.; Kumura, T. Synthesis of New Hydrotalcite-like Compounds and Their Physicochemical Properties. *Chem. Lett.* **1973**, *2*, 843–848. [CrossRef]
33. Costantino, U.; Marmottini, F.; Nocchetti, M.; Vivani, R. New Synthetic Routes to Hydrotalcite-like Compounds—Characterisation and Properties of the Obtained Materials. *Eur. J. Inorg. Chem.* **1998**, *10*, 1439–1446. [CrossRef]
34. Greenwell, H.C.; Jones, W.; Stamires, D.N.; O'Connor, P.; Brady, M.F. A One-pot Synthesis of Hybrid Organo-layered Double Hydroxide Catalyst Precursors. *Green Chem.* **2006**, *8*, 1067–1072. [CrossRef]
35. Greenwell, H.C.; Jones, W.; Rugen-Hankey, S.L.; Holliman, P.J.; Thompson, R.L. Efficient Synthesis of Ordered Organo-layered Double Hydroxides. *Green Chem.* **2010**, *12*, 688–695. [CrossRef]
36. Greenwell, H.C.; Marsden, C.C.; Jones, W. Synthesis of Organo-layered Double Hydroxides by an Environmentally Friendly Co-Hydration Route. *Green Chem.* **2007**, *9*, 1299–1307. [CrossRef]
37. Kagunya, W.; Hassan, Z.; Jones, W. Catalytic Properties of Layered Double Hydroxides and Their Calcined Derivatives. *Inorg. Chem.* **1996**, *35*, 5970–5974. [CrossRef]
38. Hernandez, M.; Lauwaert, J.; Van Der Voort, P. Recent Advances on the Utilization of Layered Double Hydroxides (LDHs) and Related Heterogeneous Catalysts in a Lignocellulosic-Feedstock Biorefinery Scheme. *Green Chem.* **2017**, *19*, 5259–5516. [CrossRef]
39. Yan, K.; Liu, Y.; Lu, Y.; Chai, J.; Sun, L. Catalytic application of layered double hydroxide-derived catalyst for the conversion of biomass-derived molecules. *Catal. Sci. Technol.* **2017**, *7*, 1622–1645. [CrossRef]
40. Roeffaers, M.B.J.; Sels, B.F.; Uji-i, H.; De Schryver, F.C.; Jacobs, P.A.; De Vos, D.E.; Hofkens, J. Spatially Resolved Observation of Crystal-Face-Dependent Catalysis by Single Turnover Counting. *Nature* **2006**, *439*, 572–575. [CrossRef] [PubMed]
41. Figueras, F.O. Base Catalysis in the Synthesis of Fine Chemicals. *Top. Catal.* **2004**, *29*, 189–196. [CrossRef]
42. Lee, D.; Park, Y.; Lee, K. Heterogeneous Base Catalysts for Transesterification in Biodiesel Synthesis. *Catal. Surv. Asia* **2009**, *13*, 63–77. [CrossRef]
43. Goswamee, R.L.; Saikia, J.; Allou, N.B. Use of Calcined Mg–Al Layered Double Hydroxides to Regulate Endocrine Disruptor Methylparaben in Excess as Adsorbent and as Control Releasing Agent in Normal Situations. *J. Environ. Chem. Eng.* **2017**, *6*, 1189–1200.
44. Guida, A.; Lhouty, M.H.; Tichit, D.; Figueras, F.; Geneste, P. Hydrotalcites as Base Catalysts. Kinetics of Claisen-Schmidt Condensation, Intramolecular Condensation of Acetonylacetone and Synthesis of Chalcone. *Appl. Catal. A Gen.* **1997**, *164*, 251–264. [CrossRef]
45. Brito, A.; Borges, M.E.; Garin, M.; Hernandez, A. Biodiesel Production from Waste Oil Using Mg–Al Layered Double Hydroxide Catalysts. *Energy Fuels* **2009**, *23*, 2952–2958. [CrossRef]
46. Choudary, B.M.; Kantam, M.L.; Reddy, C.R.V.; Rao, K.K.; Figueras, F. The first example of Michael addition catalysed by modified Mg–Al hydrotalcite. *J. Mol. Catal. A Chem.* **1999**, *146*, 279–284. [CrossRef]
47. Parida, K.; Das, J. Mg/Al Hydrotalcites: Preparation, Characterisation and Ketonisation of Acetic Acid. *J. Mol. Catal. A Chem.* **2000**, *151*, 185–192. [CrossRef]
48. Constantino, V.R.L.; Pinnavaia, T.J. Basic Properties of $Mg_{1-x}^{2+}Al_x^{3+}$ Layered Double Hydroxides Intercalated by Carbonate, Hydroxide, Chloride and Sulfate Aanions. *Inorg. Chem.* **1995**, *34*, 883–892. [CrossRef]
49. Perez-Ramirez, J.; Abello, S.; van der Pers, N.M. Influence of the divalent cation on the thermal activation and reconstruction of hydrotalcite-like compounds. *J. Phys. Chem. C* **2007**, *111*, 3642–3650. [CrossRef]
50. Tichit, D.; Gerardin, C.; Durand, R.; Coq, B. Layered Double Hydroxides: Precursors for Multifunctional Catalysts. *Top. Catal.* **2006**, *39*, 89–96. [CrossRef]
51. Constantino, V.R.L.; Pinnavaia, T.J. Structure-Reactivity Relationships for Basic Catalysts Derived from a $Mg^{2+}Al^{3+}(CO_3^{2-})$ Layered Double Hydroxide. *Catal. Lett.* **1994**, *23*, 361–367. [CrossRef]
52. Cantrell, D.G.; Gillie, L.J.; Lee, A.F.; Wilson, K. Structure-reactivity Correlations in MgAl Hydrotalcite Catalysts for Biodiesel Synthesis. *Appl. Catal. A Gen.* **2005**, *287*, 183–190. [CrossRef]

53. Cross, H.E.; Brown, D.R. Entrained Sodium in Mixed Metal Oxide Catalysts Derived from Layered Double Hydroxides. *Catal. Commun.* **2010**, *12*, 243–245. [CrossRef]
54. He, J.; Wei, M.; Li, B.; Kang, Y.; Evans, D.G.; Duan, X. Preparation of Layered Double Hydroxides. In *Layered Double Hydroxides*; Duan, X., Evans, D.G., Eds.; Springer: Berlin/Heidelberg, Germany, 2006; pp. 89–119.
55. Tichit, D.; Coq, B. Catalysis by Hydrotalcites and Related Materials. *Cattech* **2003**, *7*, 206–217. [CrossRef]
56. Hammett, L.P.; Deyrup, A.J. A series of Simple Basic Indicators. I. The Acidity Functions of Mixtures of Sulfuric and Perchloric Acids with Water. *J. Am. Chem. Soc.* **1932**, *54*, 2721–2739. [CrossRef]
57. Xie, W.L.; Peng, H.; Chen, L.G. Calcined Mg–Al Hydrotalcites as Solid Base Catalysts for Methanolysis of Soybean Oil. *J. Mol. Catal. A Chem.* **2006**, *246*, 24–32. [CrossRef]
58. Prinetto, F.; Ghiotti, G.; Durand, R.; Tichit, D. Investigation of Acid-Base Properties of Catalysts Obtained from Layered Double Hydroxides. *J. Phys. Chem. B* **2000**, *104*, 11117–11126. [CrossRef]
59. Shen, J.Y.; Kobe, J.M.; Chen, Y.; Dumesic, J.A. Synthesis and Surface Acid/Base Properties of Magnesium–Aluminum Mixed Oxides Obtained from Hydrotalcites. *Langmuir* **1994**, *10*, 3902–3908. [CrossRef]
60. Hobbs, C.; Jaskaniec, S.; McCarthy, E.K.; Downing, C.; Opelt, K.; Güth, K.; Shmeliov, A.; Mourad, M.C.D.; Mandel, K.; Nicolosi, V. Structural Transformation of Layered Double Hydroxides: An in situ TEM Analysis. *2D Mater. Appl.* **2018**, *2*, 4. [CrossRef]
61. Mahjoubi, F.Z.; Khalidi, A.; Abdennouri, M.; Barka, N. Zn–Al Layered Double Hydroxides Intercalated with Carbonate, Nitrate, Chloride and Sulphate Ions: Synthesis, Characterisation and Dye Removal Properties. *J. Taibah Univ. Sci.* **2017**, *11*, 90–100. [CrossRef]
62. Kaneyoshi, M.; Jones, W. Formation of Mg–Al Layered Double Hydroxides Intercalated with Nitrilotriacetate Anions. *J. Mater. Chem.* **1999**, *9*, 805–811. [CrossRef]
63. Hudson, M.J.; Carlino, S.; Apperley, D.C. Thermal Conversion of a Layered (Mg/Al) Double Hydroxide to the Oxide. *J. Mater. Chem.* **1995**, *5*, 323–329. [CrossRef]
64. Li, S.-S.; Jiang, M.; Jiang, T.-J.; Liu, J.-H.; Guo, Z.; Huang, X.-J. Competitive Adsorption Behavior Toward Metal Ions On Nano-Fe/Mg/Ni Ternary Layered Double Hydroxide Proved by XPS: Evidence of Selective and Sensitive Detection of Pb(II). *J. Hazardous Mater.* **2017**, *338*, 1–10. [CrossRef] [PubMed]
65. Valente, J.S.; Sanchez-Cantu, M.; Lima, E.; Figueras, F. Method for Large-Scale Production of Multimetallic Layered Double Hydroxides: Formation Mechanism Discernment. *Chem. Mater.* **2009**, *21*, 5809–5818. [CrossRef]
66. Rives, V. *Layered Double Hydroxides: Present and Future*; Nova Science Publishers: Hauppauge, NY, USA, 2001.
67. Reichle, W.T.; Kang, S.Y.; Everhardt, D.S. The Nature of the Thermal-Decomposition of a Catalytically Active Anionic Clay Mineral. *J. Catal.* **1986**, *101*, 352–359. [CrossRef]
68. Velu, S.; Suzuki, K.; Okazaki, M.; Osaki, T.; Tomura, S.; Ohashi, F. Synthesis of New Sn-incorporated Layered Double Hydroxides and their Thermal Evolution to Mixed Oxides. *Chem. Mater.* **1999**, *11*, 2163–2172. [CrossRef]
69. Zhao, Y.; Li, F.; Zhang, R.; Evans, D.G.; Duan, X. Preparation of Layered Double-Hydroxide Nanomaterials with a Uniform Crystallite Size Using a New Method Involving Separate Nucleation and Aging Steps. *Chem. Mater.* **2002**, *14*, 4286–4291. [CrossRef]
70. Sing, K.S.W.; Everett, D.H.; Haul, R.A.W.; Moscou, L.; Pierotti, R.A.; Rouquerol, J.; Siemieniewska, T. Reporting Physisorption Data for Gas Solid Systems with Special Reference to the Determination of Surface-Area and Porosity. *Pure Appl. Chem.* **1985**, *57*, 603–619. [CrossRef]
71. Kang, D.; Yu, X.; Tong, S.; Ge, M.; Zuo, J.; Cao, C.; Song, W. Performance and Mechanism of Mg/Fe Layered Double Hydroxides for Fluoride and Arsenate Removal from Aqueous Solution. *Chem. Eng. J.* **2013**, *228*, 731–740. [CrossRef]
72. Greenwell, H.C.; Stackhouse, S.; Coveney, P.V.; Jones, W. A Density Functional Theory Study of Catalytic Trans-Esterification by Tert-Butoxide Mgal Anionic Clays. *J. Phys. Chem. B* **2003**, *107*, 3476–3485. [CrossRef]
73. Shichi, T.; Takagi, K.; Sawaki, Y. Stereoselectivity Control of 2 + 2 Photocycloaddition by Changing Site Distances of Hydrotalcite Interlayers. *Chem. Commun.* **1996**, *17*, 2027–2028. [CrossRef]
74. Takagi, K.; Shichi, T.; Usami, H.; Sawaki, Y. Controlled Photocycloaddition of Unsaturated Carboxylates Intercalated in Hydrotalcite Clay Interlayers. *J. Am. Chem. Soc.* **1993**, *115*, 4339–4344. [CrossRef]
75. Zhang, A.H.; Ma, Q.S.; Wang, K.S.; Liu, X.C.; Shuler, P.; Tang, Y.C. Naphthenic Acid Removal from Crude Oil Through Catalytic Decarboxylation On Magnesium Oxide. *Appl. Catal. A Gen.* **2006**, *303*, 103–109. [CrossRef]

76. Corma, A.; Renz, M.; Schaverien, C. Coupling Fatty Acids by Ketonic Decarboxylation Using Solid Catalysts for the Direct Production of Diesel, Lubricants, and Chemicals. *ChemSusChem* **2008**, *1*, 739–741. [CrossRef] [PubMed]
77. Verziu, M.; Cojocaru, B.; Hu, J.; Richards, R.; Ciuculescu, C.; Filip, P.; Parvulescu, V.I. Sunflower and Rapeseed Oil Transesterification to Biodiesel Over Different Nanocrystalline MgO Catalysts. *Green Chem.* **2008**, *10*, 373–381. [CrossRef]
78. Na, J.G.; Yi, B.E.; Kim, J.N.; Yi, K.B.; Park, S.Y.; Park, J.H.; Ko, C.H. Hydrocarbon Production from Decarboxylation of Fatty Acid Without Hydrogen. *Catal. Today* **2010**, *156*, 44–48. [CrossRef]
79. Gaertner, C.A.; Serrano-Ruiz, J.C.; Braden, D.J.; Dumesic, J.A. Ketonization Reactions of Carboxylic Acids and Esters over Ceria–Zirconia as Biomass-Upgrading Processes. *Ind. Eng. Chem. Res.* **2010**, *49*, 6027–6033. [CrossRef]
80. Kubičková, I.; Snåre, M.; Eränen, K.; Mäki-Arvela, P.; Murzin, D. Hydrocarbons for diesel fuel via decarboxylation of vegetable oils. *Catal. Today* **2005**, *106*, 197–200. [CrossRef]
81. Anastas, P.; Warner, J. *Green Chemistry: Theory and Practice*; Oxford University Press: Oxford, UK, 2000.
82. *Clarity Chromatography Station*, Clarity Chromatography Station version 2.4.1.57; DataApex: Prague, Czech Republic, 2003.
83. *ASTM D6584-10ae1, Standard Test Method for Determination of Total Monoglyceride, Total Diglyceride, Total Triglyceride, and Free and Total Glycerin in B-100 Biodiesel Methyl Esters by Gas Chromatography*; ASTM International: West Conshohocken, PA, USA, 2010.
84. Barthomeuf, D. Conjugate Acid-base Pairs in Zeolites. *J. Phys. Chem.* **1984**, *88*, 42–45. [CrossRef]
85. Sánchez-Sánchez, M.; Blasco, T. Characterization of Zeolite Basicity Using Probe Molecules by Means of Infrared and Solid State NMR Spectroscopies. *Catal. Today* **2009**, *143*, 293–301. [CrossRef]
86. Griinert, W.; Muhler, M.; Schroder, K.; Sauer, J.; Schloegl, R. Investigations of Zeolites by Photoelectron and Ion Scattering Spectroscopy. 2. A New Interpretation of XPS Binding Energy Shifts in Zeolites. *J. Phys. Chem.* **1994**, *98*, 10920–10929. [CrossRef]